Journal of Advanced Ceramics
2021, **10**(4): 843–851
https://doi.org/10.1007/s40145-021-0478-x
ISSN 2226-4108
CN 10-1154/TQ

Research Article

Effect of anionic group $[SiO_4]^{4-}$/$[PO_4]^{3-}$ on the luminescence properties of Dy^{3+}-doped tungstate structural compounds

Ning LIU[a,b], Lefu MEI[b,*], Jianxiong BIN[b], Ze ZHANG[b], Zhijian PENG[a,*]

[a]*School of Science, China University of Geosciences (Beijing), Beijing 100083, China*
[b]*Beijing Key Laboratory of Materials Utilization of Nonmetallic Minerals and Solid Wastes, National Laboratory of Mineral Materials, School of Materials Sciences and Technology, China University of Geosciences (Beijing), Beijing 100083, China*

Received: December 15, 2020; Revised: February 27, 2021; Accepted: March 22, 2021

Abstract: Novel scheelite structures of $Li_2Ca(WO_4)_2$, $Li_2Ca_2(WO_4)(SiO_4)$, and $LiCa_2(WO_4)(PO_4)$ fluorescent materials were successfully prepared using a high-temperature solid-phase process. The compounds were characterized by X-ray diffraction and energy dispersive spectroscopy. The tests revealed that the substitution of $[WO_4]^{2-}$ by $[SiO_4]^{4-}$ or $[PO_4]^{3-}$ tetrahedron in tungstate had no significant influence on the crystal structure of the $Li_2Ca(WO_4)_2$. When Dy^{3+} ions were introduced as an activator at an optimum doping concentration of 0.08 mol%, all of the as-prepared phosphors generated yellow light emissions, and the emission peak was located close to 576 nm. Replacing $[WO_4]^{2-}$ with $[SiO_4]^{4-}$ or $[PO_4]^{3-}$ tetrahedron significantly increased the luminescence of the $Li_2Ca(WO_4)_2$ phosphors. Among them, the $LiCa_2(WO_4)(PO_4)$:0.08Dy^{3+} phosphor had the best luminescence properties, decay life (τ = 0.049 ms), and thermal stability (87.8%). In addition, the as-prepared yellow $Li_2Ca(WO_4)_2$:0.08Dy^{3+}, $Li_2Ca_2(WO_4)(SiO_4)$:0.08Dy^{3+}, and $LiCa_2(WO_4)(PO_4)$:0.08Dy^{3+} phosphor can be used to fabricate white light emitting diode (LED) devices.

Keywords: phosphors; scheelite structure; luminescence property; anion substitution

1 Introduction

Inorganic luminescent materials have historically attracted considerable attention due to their characteristics such as long decay lifetime [1], easy preparation, low toxicity, and high luminous efficiency [2–4]. Rare earth luminescent materials have considerable application potential because of their unique 4f orbit, which can be pumped to excited energy levels to emit colorful light under excitation [5,6]. Among them, the emission of Dy^{3+} is mainly from the yellow–orange region (570–600 nm) with $^4F_{9/2}\rightarrow{}^6H_{13/2}$ transition [7], and $^4F_{9/2}\rightarrow{}^6H_{15/2}$ transition at the blue region (470–500 nm) [8]. At a sufficient yellow–blue intensity ratio, Dy^{3+} can also emit white light [9]. The excitation spectrum of Dy^{3+} consists only of narrow f–f transition lines with low oscillation intensity due to the characteristics of the 300–500 nm parity selection rule (Dy^{3+} charge transfer absorption bands or $4f^8\rightarrow4f^7$ 5d bands below 200 nm). Effective energy transfer from the matrix to the Dy^{3+} ions is one of the most relevant methods to achieve efficient emission of Dy^{3+} ions in the matrix sensitization of Dy^{3+} ions [10].

* Corresponding authors.
E-mail: L. Mei, mlf@cugb.edu.cn;
Z. Peng, pengzhijian@cugb.edu.cn

The luminescent properties of phosphors are affected by the doped rare earth ions, as well as the structure and composition of the substance host [11,12]. Tungstate materials are considered to be effective self-activated fluorescent materials with high-absorption cross-sections [13,14], broadband emissions [15], and high quantum efficiency [16,17]. To fix the weak f–f transitions in trivalent rare earth ions, self-activating compounds may also serve as matrix sensitizers. The lattice of matrix material not only affects the dopant's optical transition, but also reduces its excitation energy [18]. Among various matrix materials, phosphate has a wide band gap and high efficiency, with high thermal stability and chemical durability [19,20]. Silicate has been widely studied as a satisfactory matrix for fluorescent materials due to its excellent optical properties, chemical stability, and structural diversity [21,22]. On the basis of these advantages, $[SiO_4]^{4-}$ or $[PO_4]^{3-}$ ion substitution of $[WO_4]^{2-}$ ion to synthesize a novel scheelite structural matrix in tungstate is considered to be a viable and suitable luminescent material carrier [23]. Combining the stable physical and chemical properties of the matrix materials, $Li_2Ca(WO_4)_2$:xDy^{3+}, $Li_2Ca_2(WO_4)(SiO_4)$:yDy^{3+}, and $LiCa_2(WO_4)(PO_4)$:zDy^{3+} phosphors with low energy consumption and high thermal stability were synthesized using a high-temperature solid-phase process, and the luminescence behaviors of Dy^{3+} in the three hosts were studied. To verify the effect of $[SiO_4]^{4-}$ or $[PO_4]^{3-}$ substitution on the properties of the tungstate matrix fluorescent materials and elucidate the effect of anion substitution on their crystal structures, a series of comparative experiments were conducted to evaluate the different properties after the replacement of the crystal phase and anions in the samples. The luminescence properties of the doped samples were discussed in the three modified matrices, including excitation spectrum, emission spectrum, decay time, chromaticity diagram, and luminescence mechanism of the doped ions in them. For their future practical applications, the thermal stability has also been investigated.

2 Experimental

2. 1 Material preparation

All of the as-prepared solid-solution samples were synthesized using a typical high-temperature solid-phase reaction method under air atmosphere. The initial raw materials were WO_3 (analytical reagent, AR), SiO_2 (AR), Dy_2O_3 (99.99%), $CaCO_3$ (AR), Li_2CO_3 (AR), and $(NH_4)_2HPO_4$ (AR) with excessive H_3BO_3 (AR) as flux, which were all commercially bought from Beijing Chemical Co., China. All of the initial reagents were weighed according to the stoichiometric ratios and mixed by grinding in an agate mortar for more than 10 min. The mixed powders were then calcined in a muffle furnace at 550 ℃ for 2 h, cooled to room temperature naturally, and thoroughly ground again for another 5 min. Afterwards, different anion-regulated compounds were synthesized under varying conditions. The $Li_2Ca(WO_4)_2$:xDy^{3+} samples were prepared at 1000 ℃ for 3 h in a high-temperature tube furnace at a heating rate of 5 ℃/min. The $Li_2Ca_2(WO_4)(SiO_4)$:yDy^{3+} samples were synthesized in the high-temperature tube furnace by calcining at the same heating rate to 850 ℃ for 3 h, but the $LiCa_2(WO_4)(PO_4)$:zDy^{3+} samples were calcined at 1400 ℃ for 3 h. All the three kinds of samples were then naturally cooled to room temperature and thoroughly ground in an agate mortar into fine powders for further measurements.

2. 2 Material characterization

The structural properties of the as-prepared phosphors were determined using a Bruker D8 powder X-ray diffractometer (XRD, Germany) with Cu Kα radiation (λ = 0.15406 nm) working at 40 kV and 40 mA. The step scanning rate (2θ ranging from 5° to 130°) was 2.5 s/step with a step size of 0.02°. The excitation and emission spectra of the as-prepared samples were measured using a spectrophotometer (F-4600, HITACHI, Japan) equipped with a 150 W Xe lamp operating at 400 V. The field emission scanning electron microscope (FE-SEM, Hitachi, Japan) equipped with an energy dispersive X-ray spectroscopy (EDS) system was applied to observe the morphology and measure the elemental composition of the as-prepared powders. The decay curves of the samples were recorded by a spectrofluorometer (HORIBA, Jobin Yvon FL3-21, France). A Hitachi F-4600 spectrophotometer with an automatic heating system and a self-controlled electric incinerator was used to determine the temperature-dependent photoluminescence (PL) spectrum.

2. 3 Fabrication of white light emitting diode (LED) devices

To fabricate white LED devices, the commercially available blue $BaMgAl_{10}O_{17}$:Eu^{2+} powders and yellow–

green SiAlON:Eu^{2+} powders were mixed with the as-prepared $Li_2Ca(WO_4)_2$:0.08Dy^{3+}, $Li_2Ca_2(WO_4)(SiO_4)$: 0.08Dy^{3+}, $LiCa_2(WO_4)(PO_4)$:0.08Dy^{3+}, and phosphor powders, respectively, in a mass ratio of 2:1:20. Afterwards, with Dow Corning OE6550 gel in a mass ratio of 1:1 to the above mixed powders, a 275 nm emitting LED chip was combined with the mixed powders, and then the chip was attached to an LED pedestal. Finally, the devices were dried at 150 ℃ for 1 h in air. A NOVA high sensitive spectrometer (IdeaOptics, China) was used to determine the optical properties of the fabricated white LED devices including the correlated color temperature (CCT), color render index (*Ra*), and the Commission Internationale de L'Eclairage (CIE) coordinates.

3 Results and discussion

3. 1 Crystal structure

XRD measurements were conducted to examine the phase structure and purity of the three samples. The XRD patterns of the as-obtained $Li_2Ca(WO_4)_2$:$x$$Dy^{3+}$, $Li_2Ca_2(WO_4)(SiO_4)$:$y$$Dy^{3+}$, and $LiCa_2(WO_4)(PO_4)$:$z$$Dy^{3+}$ samples are displayed in Fig. 1. It is easily seen that all the samples exhibit similar profile and the observed,

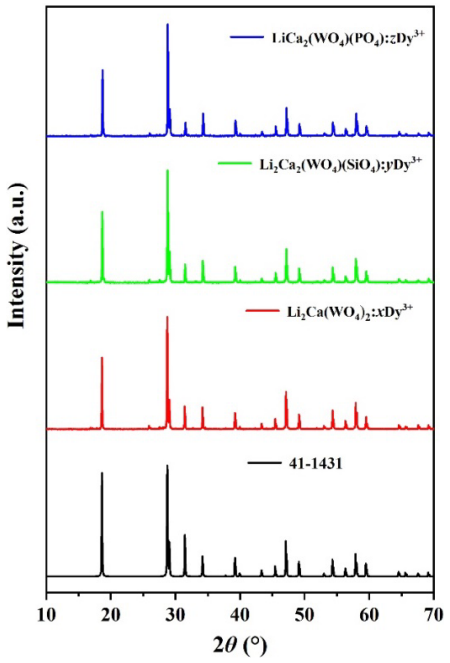

Fig. 1 XRD patterns of the as-obtained $Li_2Ca(WO_4)_2$:$x$$Dy^{3+}$, $Li_2Ca_2(WO_4)(SiO_4)$:$y$$Dy^{3+}$, and $LiCa_2(WO_4)(PO_4)$:$z$$Dy^{3+}$ samples with the standard PDF#41-1431 card ($CaWO_4$) as a reference.

coincided diffraction peaks are consistent with previous reports [24], revealing that the investigated three samples possess the same phase as tungstate-structural $CaWO_4$ (cubic structure, $I41/a$; space group No. 88) and the doping ions are successfully incorporated into the host lattices. Additionally, the few of peaks in the range of 15°–20° and 25°–30° could be attributed to the Li_2WO_4 phase (JCPDS Card No. 12-0772), but it would not affect the luminous performance of the main phase [25].

3. 2 Morphology and elemental analysis

SEM imaging and EDS analysis were carried out to observe the morphology and measure the chemical composition of the compounds prepared in this work. Figure 2(a) displays the typical SEM image of the designed $Li_2Ca_2(WO_4)(SiO_4)$ sample. As seen from Fig. 2(a), the particles in the sample could be relatively large due to their sintering during calcining. On a randomly selected large particle, EDS analysis was performed. Figure 2(b) shows the EDS spectrum by surface-point elemental analysis, and the measured corresponding elemental composition is presented in Table 1. The result indicates that except for Au from the SEM sample holder, the contents of Ca, O, W, and Si in the obtained sample are 16.2, 38.7, 36.6 and 6.07 wt%, respectively, presenting an atomic ratio of Ca:O:W:Si as 2:12:1:1.5, which are close to the stoichiometry of the designed $Li_2Ca_2(WO_4)(SiO_4)$. Figure 2(c) exhibits the EDS results by elemental mapping analysis, which further confirms the presence of Si^{4+} ions in the obtained $Li_2Ca_2(WO_4)(SiO_4)$ sample. Moreover, EDS mapping revealed that the distributions of the elements including Si in the sample were all very uniform, indicating that $[SiO_4]^{4-}$ successfully replaced the $[WO_4]^{2-}$ position. All these results demonstrate that the as-obtained sample is the $Li_2Ca_2(WO_4)(SiO_4)$ phosphor designed in this work. Similar SEM imaging and EDS analysis were also performed on the designed $LiCa_2(WO_4)(PO_4)$ compounds. Figure 2(d) shows typical SEM image on the $Li_2Ca_2(WO_4)(PO_4)$ sample. Similarly, large particles were also observed in the obtained $Li_2Ca_2(WO_4)(PO_4)$ sample due to the same reason of sintering as that in $Li_2Ca_2(WO_4)(SiO_4)$. Figure 2(e) exhibits the EDS spectrum by surface-point elemental analysis, and the measured corresponding elemental composition is presented in Table 2. The measured contents of Ca, O, W, and P in the obtained $LiCa_2(WO_4)(PO_4)$ sample are 16.0, 35.8, 34.3 and 8.58 wt%, respectively, presenting an atomic ratio of

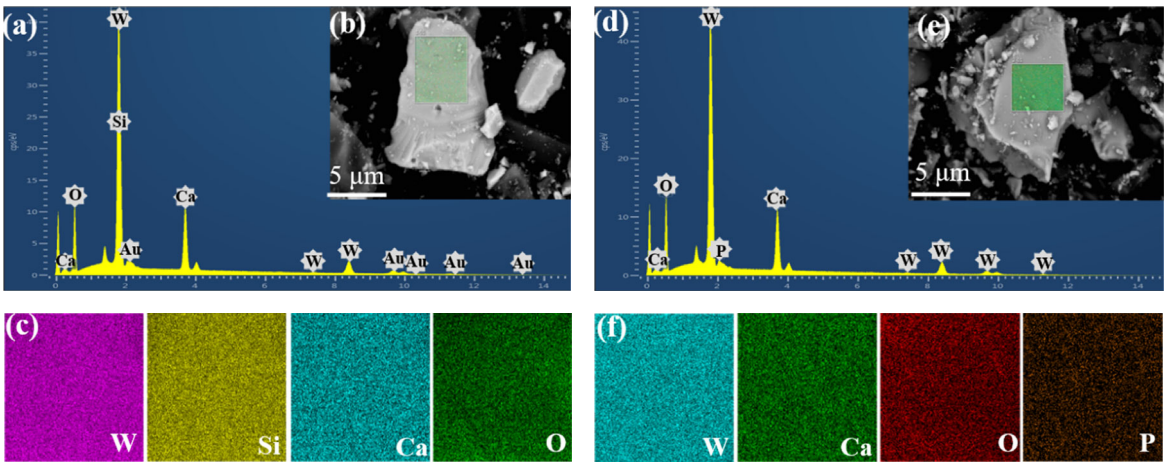

Fig. 2 (a) EDS spectrum, (b) SEM image, and (c) elemental mapping images of $Li_2Ca_2(WO_4)(SiO_4)$. (d) EDS spectrum, (e) SEM image, and (f) elemental mapping images of $LiCa_2(WO_4)(PO_4)$.

Table 1 Elemental analysis of the as-obtained $Li_2Ca_2(WO_4)(SiO_4)$ sample (Ca, O, W, Si)

Element	Measured content (wt%)	Theoretical content (wt%)
Ca	16.2	18.44
O	38.7	29.51
W	36.6	42.37
Si	6.07	6.48

Table 2 Elemental analysis of the as-obtained $LiCa_2(WO_4)(PO_4)$ sample (Ca, O, W, P)

Elements	Measured content (wt%)	Theoretical content (wt%)
Ca	16.0	18.62
O	35.8	29.79
W	34.3	42.77
P	8.58	7.21

Ca:O:W:P as 2:11.5:1:1.4, which are also very close to their theoretical composition of the designed compound, confirming the successful synthesis of $LiCa_2(WO_4)(PO_4)$. Furthermore, as demonstrated in Fig. 2(f), the presence of elements such as Ca, O, W, P, and Au was detected by EDS mapping in the $LiCa_2(WO_4)(PO_4)$ sample, and all of them were also uniform. The findings showed that, except for Au from the SEM sample holder, no additional impurity elements were detected. And the elements were evenly dispersed over the sample, suggesting that $[PO_4]^{4-}$ also successfully replaced the $[WO_4]^{2-}$ position, and the sample prepared in this work was indeed the as-expected $LiCa_2(WO_4)(PO_4)$ compound.

In a word, XRD, SEM, and EDS analyses clearly demonstrated that the prepared $Li_2Ca_2(WO_4)(SiO_4)$ and $LiCa_2(WO_4)(PO_4)$ samples had a scheelite structural matrix [26].

3.3 Energy transfer processes involved in $Li_2Ca_2(WO_4)(SiO_4):yDy^{3+}$ and $LiCa_2(WO_4)(PO_4):zDy^{3+}$ phosphors

As an important activator, Dy^{3+} ions have been studied in detail in several matrices [27,28]. For scheelite structural matrices, Dy^{3+} ions can also be incorporated into the crystal lattice as an effective activator. The curves of the characteristic yellow emission peak (576 nm) and PL emission spectrum of the $Li_2Ca_2(WO_4)(SiO_4):yDy^{3+}$ and $LiCa_2(WO_4)(PO_4):zDy^{3+}$ phosphors excited by 353 nm light with a Dy^{3+} ion doping concentration are shown in Figs. 3(a) and 3(b). Since the Dy^{3+} ion 4f–4f allowed transitions [29], the photoluminescence excitation spectra of the samples contained many peaks in the range of 200–450 nm, including broadband emission peaks appearing at approximately 228, 327, 353, 366, and 388 nm. At 353 nm excitation, the emission spectra of the $Li_2Ca_2(WO_4)(SiO_4):yDy^{3+}$ and $LiCa_2(WO_4)(PO_4):zDy^{3+}$ consisted of characteristic electronic transitions of Dy^{3+} ions corresponding to the blue emission of the magnetic dipole $^4F_{9/2}\rightarrow{}^6H_{15/2}$ (478 and 488 nm) transitions. The yellow emission demonstrated the electrical dipole $^4F_{9/2}\rightarrow{}^6F_{13/2}$ (576 nm) transitions. The energy difference between $^4F_{9/2}$ and $^6F_{3/2}$ is close to the energy difference between $^6H_{15/2}$ and $^6H_{9/2}$, which usually leads to cross-relaxation of the resonance energy transfer process: $Dy^{3+}(^4F_{9/2})+Dy^{3+}(^6H_{15/2})\rightarrow Dy^{3+}(^6F_{3/2})+Dy^{3+}(^6H_{9/2})$. As shown in Figs. 3(a) and 3(b), the emission intensity of the $^4F_{9/2}\rightarrow{}^6F_{13/2}$ transition first increased as the Dy^{3+} concentration increased, and then began to decrease at a concentration of 0.08 mol% because of the effective concentration at 353 nm excitation. Figure 4 compares

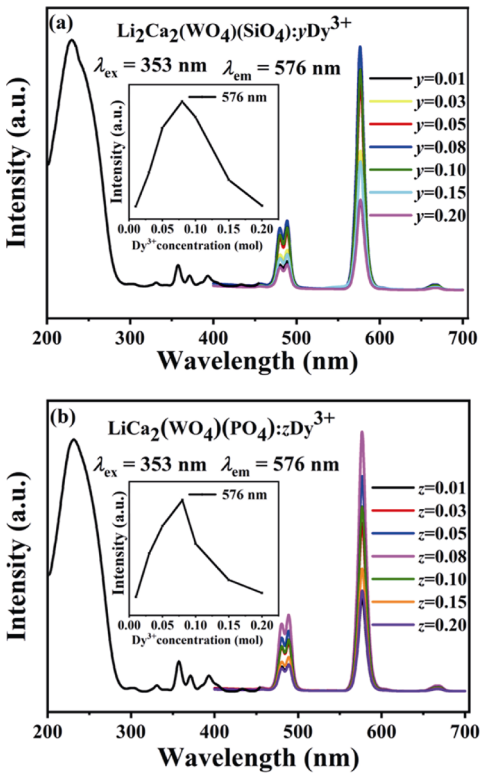

Fig. 3 Excitation and emission spectra of the as-obtained samples: (a) $Li_2Ca_2(WO_4)(SiO_4):yDy^{3+}$ and (b) $LiCa_2(WO_4)(PO_4):zDy^{3+}$, in which the insets show their corresponding dependence of PL intensity on Dy^{3+} transition.

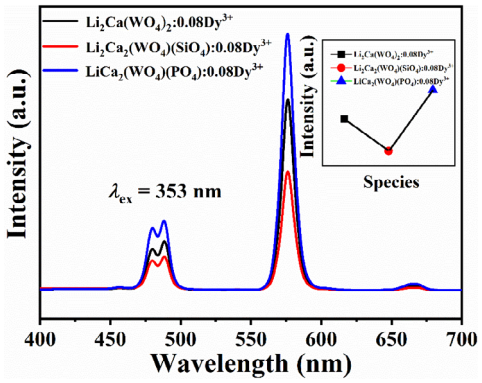

Fig. 4 PL spectra of the $Li_2Ca(WO_4)_2$:0.08Dy^{3+}, $Li_2Ca_2(WO_4)(SiO_4)$:0.08Dy^{3+}, and $LiCa_2(WO_4)(PO_4)$:0.08Dy^{3+} samples, in which the inset shows the corresponding dependence of PL intensity on Dy^{3+} transition.

the emission spectra of the $Li_2Ca(WO_4)_2$:0.08Dy^{3+}, $Li_2Ca_2(WO_4)(SiO_4)$:0.08Dy^{3+}, and $LiCa_2(WO_4)(PO_4)$:0.08Dy^{3+} samples excited by 353 nm light. As shown in the inset of Fig. 3(b), the $LiCa_2(WO_4)(PO_4)$:0.08Dy^{3+} had the best luminescence intensity, indicating that $[PO_4]^{3-}$ ion replacement $[WO_4]^{2-}$ would substantially improve the performance of tungstate matrix fluorescent materials.

3.4 Effect of $[SiO_4]^{4-}$ and $[PO_4]^{3-}$ substituting $[WO_4]^{2-}$ ions on the thermal stability of phosphors

In the practical applications of high-power solid state lighting, thermal stability is an important parameter to be considered [30–32]. So the thermal stability of the as-obtained $Li_2Ca(WO_4)_2$:0.08Dy^{3+}, $Li_2Ca_2(WO_4)(SiO_4)$:0.08Dy^{3+}, and $LiCa_2(WO_4)(PO_4)$:0.08Dy^{3+} samples was evaluated according to their temperature dependence. The emission spectrum obtained by using 353 nm wavelength light was applied to produce excitation light in a temperature range of 30–300 ℃. Figure 5 clearly shows the dependence of the luminescence

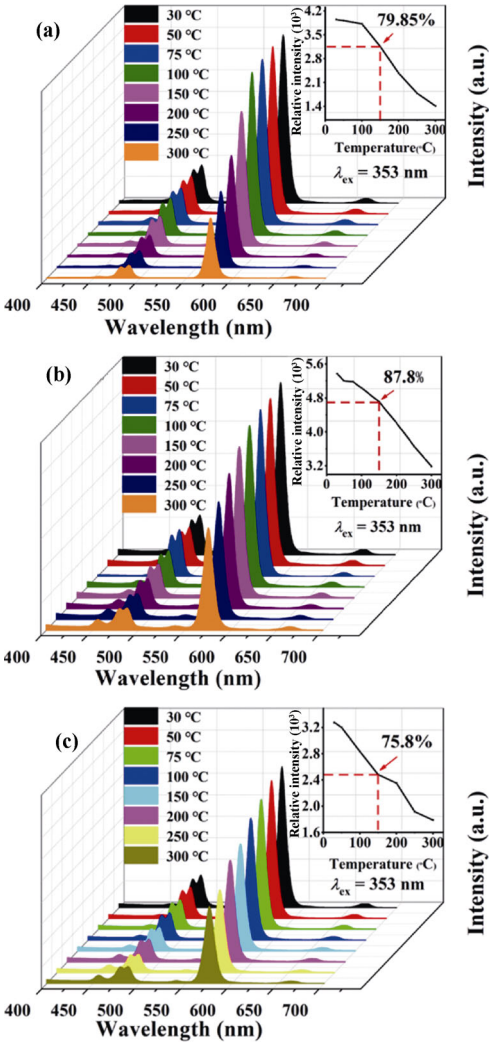

Fig. 5 PL spectra (λ_{ex} = 353 nm) of the as-obtained samples: (a) $Li_2Ca(WO_4)_2$:0.08Dy^{3+}, (b) $Li_2Ca_2(WO_4)(SiO_4)$:0.08Dy^{3+}, and (c) $LiCa_2(WO_4)(PO_4)$:0.08Dy^{3+} at different temperatures in the range of 30–300 ℃, in which their corresponding insets show the dependence of PL intensity on Dy^{3+} transition.

intensity of the Dy^{3+} ions (576 nm) on temperatures. As the temperature increased, the luminescence intensity gradually decreased and thermal quenching occurred. The changes in the luminescence intensity of the three phosphors differed from each other, indicating that the thermal stability of tungsten fluorescent materials could be significantly influenced by the substitution of anions [33]. When the temperature increased to 150 ℃, the luminescence intensity of the Dy^{3+} ions in the obtained $Li_2Ca(WO_4)_2$:0.08Dy^{3+}, $Li_2Ca_2(WO_4)(SiO_4)$:0.08Dy^{3+}, and $LiCa_2(WO_4)(PO_4)$:0.08Dy^{3+} samples were 79.85%, 75.85%, and 87.8% of their corresponding original values, respectively, indicating that they all had relatively high thermal stability. Moreover, the $LiCa_2(WO_4)(PO_4)$:0.08Dy^{3+} sample was less affected compared with the other two samples by the temperature changes, showing that it had the highest thermal stability among all the three fluorescent samples.

3. 5 Fluorescence lifetime analysis

We further investigated the effect of anion substitution on the luminescence properties and fluorescence lifetime of the scheelite structural compounds [34,35]. According to the recorded experimental data, the attenuation curves of the three compounds exhibited a second-order exponential decay that can be fitted into the following equation [36]:

$$I_{(t)} = I_0 + A_1 \exp(-t/t_1) + A_2 \exp(-t/t_2) \quad (1)$$

where $I_{(t)}$ is the luminescence intensity, I_0 denotes the initial integrated emission intensity, A_1 and A_2 are the fitting parameters, t is the time, and τ_1 and τ_2 are the lifetime of the exponential components, respectively. The average decay time τ* is calculated by using the following equation:

$$\tau^* = (A_1\tau_1^2 + A_2\tau_2^2)/(A_1\tau_1 + A_2\tau_2) \quad (2)$$

In this work, the as-obtained $Li_2Ca(WO_4)_2$:0.08Dy^{3+}, $Li_2Ca_2(WO_4)(SiO_4)$:0.08Dy^{3+}, and $LiCa_2(WO_4)(PO_4)$:0.08Dy^{3+} samples (λ_{ex} = 353 nm and λ_{em} = 576 nm) were tested for fluorescence decay life. Figure 6 shows that the τ* of the $Li_2Ca(WO_4)_2$:0.08Dy^{3+} phosphor emission was 0.032 ms. After $[SiO_4]^{4-}$ or $[PO_4]^{3-}$ replaces $[WO_4]^{2-}$, the fluorescence lifetime τ values of the obtained $Li_2Ca_2(WO_4)(SiO_4)$:0.08Dy^{3+} and $LiCa_2(WO_4)(PO_4)$:0.08Dy^{3+} samples were 0.024 and 0.049 ms, respectively. As expected, the $LiCa_2(WO_4)(PO_4)$:0.08Dy^{3+} sample has the longest fluorescence lifetime, which corresponds to the variations in PL spectrum and thermo-stability previously described in Ref. [37].

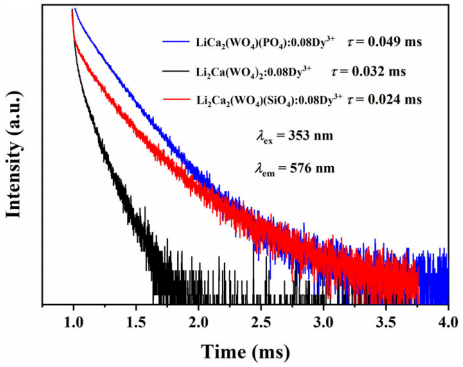

Fig. 6 Decay curves and lifetime (τ) of the as-obtained samples $Li_2Ca(WO_4)_2$:0.08Dy^{3+}, $Li_2Ca_2(WO_4)(SiO_4)$:0.08Dy^{3+}, and $LiCa_2(WO_4)(PO_4)$:0.08Dy^{3+} (λ_{em} = 576 nm) after the pulsed excitation (λ_{ex} = 353 nm) at room temperature.

3. 6 CIE spectrum coordination

Figure 7(a) shows the CIE chromaticity coordinate diagrams of the $Li_2Ca(WO_4)_2$:0.08Dy^{3+}, $Li_2Ca_2(WO_4)(SiO_4)$:0.08Dy^{3+}, and $LiCa_2(WO_4)(PO_4)$:0.08Dy^{3+} samples, and their corresponding photographs. The calculations demonstrated that the CIE chromaticity coordinates of the $Li_2Ca(WO_4)_2$:0.08Dy^{3+}, $Li_2Ca_2(WO_4)(SiO_4)$:0.08Dy^{3+}, and $LiCa_2(WO_4)(PO_4)$:0.08Dy^{3+} phosphors were (0.4053, 0.4523), (0.3892 0.4215), and (0.4124, 0.4603), respectively, corresponding to the yellow light area. In these systems, when $[SiO_4]^{4-}$ or $[PO_4]^{3-}$ replaced $[WO_4]^{2-}$, the CIE chromaticity coordinates changed slightly, which was not large because the luminescent color of the fluorescent materials was primarily determined by the type of the doped rare earth ions [38]. Therefore, yellow light-emitting phosphors that are effectively excited by the near-ultraviolet light chip could be obtained by doping the aforementioned matrix material with Dy^{3+} ions.

To evaluate the potential applications of the present three kinds of fluorescent materials as yellow phosphors for white LEDs, the as-obtained $Li_2Ca(WO_4)_2$:0.08Dy^{3+}, $Li_2Ca_2(WO_4)(SiO_4)$:0.08Dy^{3+}, and $LiCa_2(WO_4)(PO_4)$:0.08Dy^{3+} phosphors were used to fabricate white light LED prototypes, which are named as LED1, LED2, and LED3, respectively. As seen from Fig. 7(b), bright white light can be clearly observed with the as-fabricated devices. Among them, the LED1 exhibited a bright white light with a CCT = 8095 K, *Ra* = 47, and the CIE coordinates of (0.2776, 0.3536); the LED2 displayed a bright white light with a CCT =7766 K, *Ra* = 55, and the CIE coordinates of (0.2848, 0.3495); and the LED3 also presented a bright white light with a CCT = 6291 K, *Ra* = 50, and the CIE coordinates of (0.3145, 0.3477).

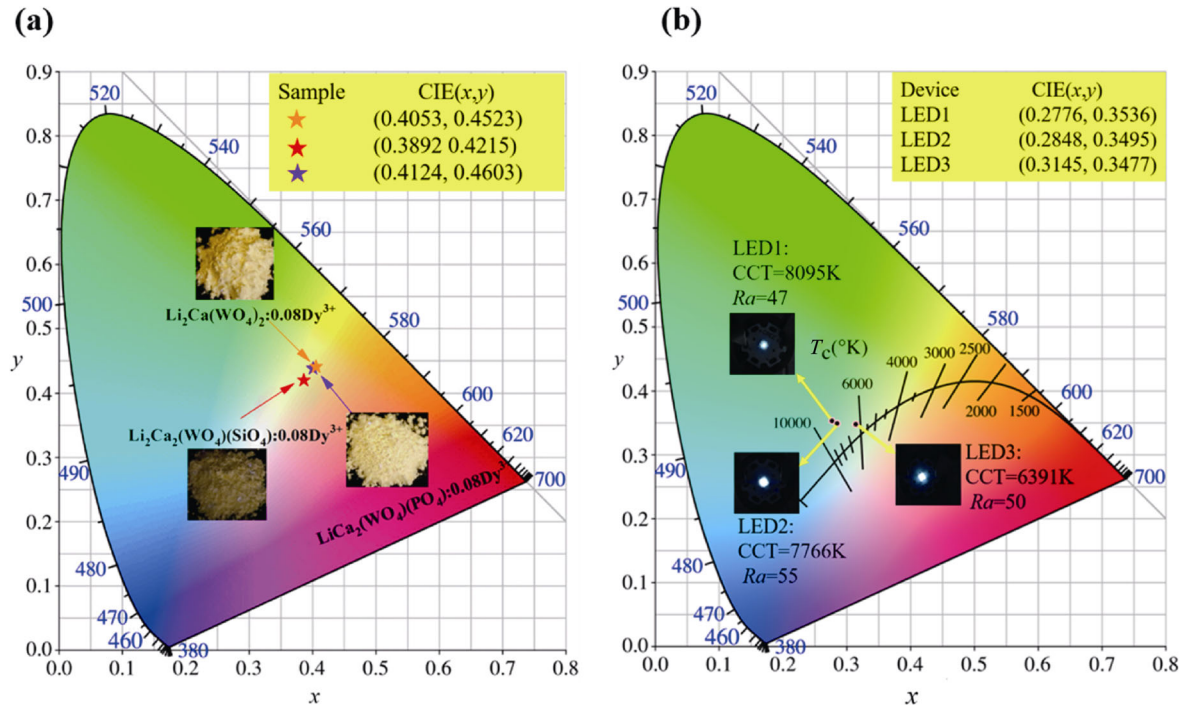

Fig. 7 (a) CIE color coordinates for the as-obtained samples $Li_2Ca(WO_4)_2$:0.08Dy^{3+} (orange star), $Li_2Ca_2(WO_4)(SiO_4)$:0.08Dy^{3+} (red star), and $LiCa_2(WO_4)(PO_4)$:0.08Dy^{3+} (purple star) at room temperature. The results are calculated by using the emission spectra under 353 nm excitation. (b) The CIE chromaticity diagram and corresponding CCT and *Ra* values of the three fabricated white light LED devices.

All these results reveal that the as-prepared yellow phosphors might be promising candidates for white LED luminescent materials.

4 Conclusions

Three Dy^{3+}-doped scheelite structural $Li_2Ca(WO_4)_2$:0.08Dy^{3+}, $Li_2Ca_2(WO_4)(SiO_4)$:0.08Dy^{3+}, and $LiCa_2(WO_4)(PO_4)$:0.08Dy^{3+} phosphors were successfully prepared through high-temperature solid-phase process. The prepared phosphors had a wide excitation band in 320–430 nm, which could be matched with the commercially available LED chips. These phosphors mainly emit yellow light peaks at 576 nm, and the optimal doping concentration was determined to be 0.08 mol%. When $[SiO_4]^{4-}$ or $[PO_4]^{3-}$ replaced $[WO_4]^{2-}$, the luminescent properties, thermal stability, and lifetime decay curves of the phosphors have been significantly improved. Finally, all the three phosphors can be used to fabricate white light LED devices, in which the $LiCa_2(WO_4)(PO_4)$:0.08Dy^{3+} phosphor has the best performance. All these results reveal that the as-prepared yellow phosphors might be promising candidates for white LED luminescent materials.

Acknowledgements

This work was supported by the National Natural Science Foundations of China (Grant Nos. 51872269 and 51672257) and the Fundamental Research Funds for the Central Universities (Grant Nos. 2652018305 and 2652017335).

References

[1] Fu ZY, Wang K, Zou B. Recent advances in organic pressure-responsive luminescent materials. *Chin Chem Lett* 2019, **30**: 1883–1894.

[2] Zhou ZP, Yu YS, Liu XT, *et al*. Luminescence enhancement of $CaMoO_4$:Eu^{3+} phosphor by charge compensation using microwave sintering method. *J Adv Ceram* 2015, **4**: 318–325.

[3] Wang X, Li XP, Shen RS, *et al*. Optical transition and luminescence properties of Sm^{3+}-doped $YNbO_4$ powder phosphors. *J Am Ceram Soc* 2020, **103**: 1037–1045.

[4] Wei YL, Su CH, Zhang HB, *et al*. Color-tunable up-conversion emission from Yb^{3+}/Er^{3+}/Tm^{3+}/Ho^{3+} codoped $KY(MoO_4)_2$ microcrystals based on energy transfer. *Ceram Int* 2016, **42**: 4642–4647.

[5] Jin C, Zhang J. Upconversion luminescence of $Ca_2Gd_8(SiO_4)_6O_2$:Yb^{3+}–Tm^{3+}–Tb^{3+}/Eu^{3+} phosphors for optical temperature sensing. *Opt Laser Technol* 2019, **115**: 487–492.

[6] Que MD, Ci ZP, Wang YH, *et al*. Synthesis and luminescent properties of $Ca_2La_8(GeO_4)_6O_2$:RE^{3+} (RE^{3+}=Eu^{3+}, Tb^{3+}, Dy^{3+}, Sm^{3+}, Tm^{3+}) phosphors. *J Lumin* 2013, **144**: 64–68.

[7] Ferhi M, Toumi S, Horchani-Naifer K, *et al*. Single phase $GdPO_4$:Dy^{3+} microspheres blue, yellow and white light emitting phosphor. *J Alloys Compd* 2017, **714**: 144–153.

[8] Wang GQ, Gong XH, Chen YJ, *et al*. Synthesis and photoluminescence properties of near-UV pumped yellow-emitting $Li_3Ba_2La_3(WO_4)_8$:Dy^{3+} phosphors. *Opt Mater* 2014, **36**: 1255–1259.

[9] Martínez-Martínez R, Lira AC, Speghini A, *et al*. Blue-yellow photoluminescence from Ce^{3+}→Dy^{3+} energy transfer in HfO_2:Ce^{3+} films deposited by ultrasonic spray pyrolysis. *J Alloys Compd* 2011, **509**: 3160–3165.

[10] Sabalisck NP, Lahoz F, González-Silgo MC, *et al*. Control of the luminescent properties of $Eu_{2-x}Dy_x(WO_4)_3$ solid solutions for scintillator applications. *J Alloys Compd* 2017, **726**: 796–802.

[11] Li LL, Wu HY. Host composition dependent tuneable morphology and luminescent property of the $Ca_xSr_yBa_{1-x-y}WO_4$:RE^{3+} (RE = Pr, Ho, and Er) phosphors. *J Alloys Compd* 2017, **702**: 106–119.

[12] Liang J, Devakumar B, Sun LL, *et al*. Full-visible-spectrum lighting enabled by an excellent cyan-emitting garnet phosphor. *J Mater Chem C* 2020, **8**: 4934–4943.

[13] Guo WL, Tian Y, Huang P, *et al*. Color tunable luminescence in novel $Li_3Ba_2Y_3(WO_4)_8$:Tb^{3+},Eu^{3+} phosphor for white LEDs. *Ceram Int* 2016, **42**: 5427–5432.

[14] Kasprowicz D, Brik MG, Majchrowski A, *et al*. Spectroscopic properties of $KGd(WO_4)_2$ single crystals doped with Er^{3+}, Ho^{3+}, Tm^{3+} and Yb^{3+} ions: Luminescence and micro-Raman investigations. *J Alloys Compd* 2013, **577**: 687–692.

[15] Yu XC, Gao ML, Li JX, *et al*. Near infrared to visible upconversion emission in Er^{3+}/Yb^{3+} co-doped $NaGd(WO_4)_2$ nanoparticles obtained by hydrothermal method. *J Lumin* 2014, **154**: 111–115.

[16] Wang L, Guo WL, Tian Y, *et al*. High luminescent brightness and thermal stability of red emitting $Li_3Ba_2Y_3(WO_4)_8$: Eu^{3+} phosphor. *Ceram Int* 2016, **42**: 13648–13653.

[17] Kasprowicz D, Głuchowski P, Brik MG, *et al*. Visible and near-infrared up-conversion luminescence of $KGd(WO_4)_2$ micro-crystals doped with Er^{3+}, Tm^{3+}, Ho^{3+} and Yb^{3+} ions. *J Alloys Compd* 2016, **684**: 271–281.

[18] Bin JX, Liu HK, Mei LF, *et al*. Multi-color luminescence evolution and efficient energy transfer of scheelite-type $LiCaGd(WO_4)_3$:Ln^{3+} (Ln = Eu, Dy, Tb) phosphors. *Ceram Int* 2019, **45**: 1837–1845.

[19] Lim H, Lim J, Jang S, *et al*. Emissions of Er^{3+} and Yb^{3+} co-doped $SrZrO_3$ nanocrystals under near-infrared and near-ultraviolet excitations. *J Adv Ceram* 2020, **9**: 413–423.

[20] Zhang YY, Mei LF, Liu HK, *et al*. Dysprosium doped novel apatite-type white-emitting phosphor $Ca_9La(PO_4)_5(GeO_4)F_2$ with satisfactory thermal properties for *n*-UV *w*-LEDs. *Dyes Pigments* 2017, **139**: 180–186.

[21] Chartier A, Meis C, Gale JD. Computational study of Cs immobilization in the apatites $Ca_{10}(PO_4)_6F_2$, $Ca_4La_6(SiO_4)_6F_2$ and $Ca_2La_8(SiO_4)_6O_2$. *Phys Rev B* 2001, **64**: 085110.

[22] Liu HK, Mei LF, Liao LB, *et al*. Strategy for realizing ratiometric optical thermometry via efficient Tb^{3+}–Mn^{2+} energy transfer in novel apatite-type phosphor $Ca_9Tb(PO_4)_5(SiO_4)F_2$. *J Alloys Compd* 2019, **770**: 1237–1243.

[23] Liu HK, Liao LB, Guo QF, *et al*. $Ca_9La(PO_4)_5(SiO_4)Cl_2$: Dy^{3+}: A white-emitting apatite-type phosphor pumped for *n*-UV *w*-LEDs. *J Lumin* 2017, **181**: 407–410.

[24] Wen DW, Feng JJ, Li JH, *et al*. K2Ln$(PO_4)(WO_4)$:Tb^{3+}, Eu^{3+} (Ln = Y, Gd and Lu) phosphors: Highly efficient pure red and tuneable emission for white light-emitting diodes. *J Mater Chem C* 2015, **3**: 2107–2114.

[25] Zhu H, Liang CP, Huang WG. Crystal structure and luminescent properties of Li^+ ions doped double tungstate $KEu(WO_4)_2$ red emitting phosphors. *Phys B*: *Condens Matter* 2020, **582**: 411999.

[26] Sun LL, Devakumar B, Liang J, *et al*. A broadband cyan-emitting $Ca_2LuZr_2(AlO_4)_3$:Ce^{3+} garnet phosphor for near-ultraviolet-pumped warm-white light-emitting diodes with an improved color rendering index. *J Mater Chem C* 2020, **8**: 1095–1103.

[27] Kershi RM, Ali FM, Sayed MA. Influence of rare earth ion substitutions on the structural, optical, transport, dielectric, and magnetic properties of superparamagnetic iron oxide nanoparticles. *J Adv Ceram* 2018, **7**: 218–228.

[28] Yuan N, Liu DY, Yu XC, *et al*. A biological nano-thermometer based on ratiometric luminescent Er^{3+}/Yb^{3+}-codoped $NaGd(WO_4)_2$ nanocrystals. *Mater Lett* 2018, **218**: 337–340.

[29] Vijayakumar R, Guo H, Huang XY. Energy transfer and color-tunable luminescence properties of Dy^{3+} and Eu^{3+} co-doped $Na_3Sc_2(PO_4)_3$ phosphors for near-UV LED-based warm white LEDs. *Dyes Pigments* 2018, **156**: 8–16.

[30] Guo Y, Moon BK, Choi BC, *et al*. Multi-wavelength excited white-emitting $K_2Gd_{1-x}(PO_4)(WO_4)$:xDy^{3+} phosphors with satisfactory thermal properties for UV-LEDs. *RSC Adv* 2017, **7**: 23083–23092.

[31] Liu HK, Liao LB, Guo QF, *et al*. Synthesis and photoluminescence properties of Dy^{3+} doped white-emitting phosphor $Sr_9La(PO_4)_3(SiO_4)Cl_2$:$Dy^{3+}$. *Nanosci Nanotechnol Lett* 2017, **9**: 252–255.

[32] Wu XY, Liang YJ, Liu SQ, *et al*. Investigation of the luminescence properties and thermal stability of dysprosium, terbium, and europium ions singly- and co-doped strontium yttrium borate phosphors. *Spectrosc Lett* 2017, **50**: 48–54.

[33] Lima NA, Alencar LDS, Siu-Li M, *et al*. $NiWO_4$ powders prepared via polymeric precursor method for application as ceramic luminescent pigments. *J Adv Ceram* 2020, **9**: 55–63.

[34] Huang XY, Li B, Guo H, *et al*. Molybdenum-doping-induced photoluminescence enhancement in Eu^{3+}-activated $CaWO_4$ red-emitting phosphors for white light-emitting diodes. *Dyes Pigments* 2017, **143**: 86–94.

[35] Huang XY, Liang J, Rtimi S, *et al*. Ultra-high color rendering warm-white light-emitting diodes based on an efficient green-emitting garnet phosphor for solid-state lighting. *Chem Eng J* 2021, **405**: 126950.

[36] Liu N, Si JY, Cai GM, *et al*. Crystal structure, luminescence properties and energy transfer of Eu^{3+}/Dy^{3+} doped $GdNbTiO_6$ broad band excited phosphors. *RSC Adv* 2016, **6**: 50797–50807.

[37] Wu YH, Yang FG, Yan FP. Warm-white light performance of Dy^{3+},Eu^{3+}:$NaLa(WO_4)_2$ phosphors excited with a 450-nm LED. *J Am Ceram Soc* 2019, **102**: 7347–7354.

[38] Zhou ZP, Yu YS, Liu XT, *et al*. Luminescence enhancement of $CaMoO_4$:Eu^{3+} phosphor by charge compensation using microwave sintering method. *J Adv Ceram* 2015, **4**: 318–325.